Padé-Laplace method for analysis of fluorescence intensity decay

Zeljko Bajzer, Andrew C. Myers, Salah S. Sedarous, and Franklyn G. Prendergast
Department of Biochemistry and Molecular Biology, Mayo Foundation, Rochester, Minnesota 55905

ABSTRACT This novel approach to the analysis of multiexponential functions is based on the combined use of the Laplace transform and Padé approximants (Yeramian, E., and P. Claverie. 1987. *Nature (Lond.)*. 326:169–174). It is similar in principle to the well-known Isenberg method of moments (Isenberg, I. 1983. *Biophys. J.* 43:141–148) traditionally applied to the analysis of fluorescence decay. The advantage of the Padé-Laplace method lies in its ability to detect the number of components in a multiexponential function as well as their parameters. In this paper we modified the original method so that it can be applied to the analysis of multifrequency phase/modulation measurements of fluorescence decay. The method was tested first on simulated data. It afforded recovery up to four distinct lifetime components (and their fractional contributions). In the case of simulated data corresponding to continuous lifetime distributions (nonexponential decay), the results of the analysis by the Padé-Laplace method indicated the absence of discrete exponential components. The method was also applied to real phase/modulation data gathered on known fluorophores and their mixtures and on tryptophan fluorescence in phospholipase A_2. The lifetime and fraction recoveries were consistent with those obtained from standard methods involving nonlinear least-square fitting.

1. INTRODUCTION

A wide variety of methods exists for the analysis of fluorescence intensity decays whether these are measured by the use of time resolved single photon counting (1–6) or by multifrequency phase fluorometry (7–9). Generally, the methods of analysis for either type of data have relied on the use of nonlinear regression techniques. Lately, a more sophisticated approach to the analysis of fluorescence intensity decays has been developed exploiting global analysis (10–15) for the reduction of both photon counting and multifrequency data. The results with global analysis have already been impressive even though the method is still under active development. In general, however, if the fluorescence decay is monoexponential, the analysis of either time correlated single photon counting or multifrequency phase fluorometry data is usually straightforward. Problems frequently arise when the fluorescence decay is not monoexponential as the decision must then be made whether the decay should be viewed as simply a sum of exponentials, or is best considered to be nonexponential.

For studies of the fluorescence of peptides and proteins the problem has become particularly important since the observation that even when there is a single fluorophore, e.g., a single tryptophan residue, the fluorescence decay can seldom be described as monoexponential (for review see reference 13). Sometimes as many as three exponential terms are needed to provide a good fit to the data (14, 15). As noted earlier, in such situations one must ask whether the decay process should be resolved into a set of exponentials, whether the decay is nonexponential, or whether the decay ought to be interpreted in terms of a continuous distribution (15–17). It is important that the appropriate distinction be made because the inferences which one might draw regarding the physical basis for the observed fluorescence decays are very dependent on the choice one makes regarding the form of the decay process. However, it is by no means clear just how such a decision between the "standard" approach to analysis, i.e., in terms of exponential decay forms and, say, a distribution model should be made.

Yeramian and Claverie (18) have described an interesting approach to the evaluation of decay processes which relies on the use of Padé approximants (19, 20). The latter have long been used in particle and nuclear physics (e.g., 21, 22). The method of Yeramian and Claverie offers a useful opportunity for the examination of fluorescence intensity decays because it does not rely on standard statistical procedures to arrive at a conclusion as to whether a decay process is or is not exponential in form. In this paper we describe the development and

Dr. Bajzer's permanent address is Rudjer Bošković Institute, Zagreb, Croatia, Yugoslavia.

0006-3495/89/07/79/15 $2.00

implementation of the Padé-Laplace (PL) formalism for the analysis of multifrequency phase fluorometry data. In particular, we wished to determine the degree of consonance between the fluorescence decay parameters obtained by use of the PL method and those calculated by the use of nonlinear regression techniques. We measured the fluorescence lifetimes of several well-characterized, "simple" fluorophores and of a protein bearing a single tryptophan; the fluorescence intensity decay of the tryptophan in this protein is known from other reported data to be distinctly multiexponential (14, 15). The data have shown that the PL method generally yields results which are essentially identical to those found by use of nonlinear regression techniques.

2. THEORY

2.1 Padé-Laplace method

Let us assume that the observed signal $S(t), t \geq 0$ sampled at $t_j, j = 1, \ldots, m$ can be represented by multiexponential function $f(t)$:

$$f(t) = \sum_{k=1}^{n} C_k e^{\mu_k t} \tag{1}$$

$$S(t) = f(t) + n(t), \quad t = t_j. \tag{2}$$

$n(t)$ represents the instrumental noise. The parameters C_k and μ_k are unknown as well as the number of exponential components. The first step in the Padé-Laplace method is to apply Laplace transformation to $f(t)$,

$$\tilde{f}(p) = \mathcal{L}[f](p) = \int_0^\infty e^{-pt} f(t)\, dt, \tag{3}$$

obtaining

$$\tilde{f}(p) = \sum_{k=1}^{n} \frac{C_k}{p - \mu_k} = \frac{\sum_{r=1}^{n-1} u_r p^r}{\sum_{r=1}^{n} v_r p^r} \tag{4}$$

The integral in Eq. 3 is convergent for all complex p satisfying $Re(p) > Sup_k\,[Re(\mu_k)], k = 1, \ldots, n$ and the function $\tilde{f}(p)$ can be analytically continued to the whole complex p plane. The unknown parameters C_k and μ_k are simply poles and corresponding residues of $\tilde{f}(p)$. The function $\tilde{f}(p)$ can be calculated by numerical integration,

$$\tilde{f}(p) = \tilde{S}(p) + e_m(p), \quad \tilde{S}(p) = \sum_{j=1}^{m} w_j S(t_j) e^{-pt_j}. \tag{5}$$

Here the weights w_j and t_j are specific to the numerical integration used. The error $e_m(p)$ depends on the method of numerical integration and on the noise $n(t)$. The function $\tilde{S}(p)$ is analytic in the complex plane p, and can be represented at a particular p_0 by its Taylor series:

$$\tilde{S}(p) = \sum_{i=0}^{\infty} d_i (p - p_0)^i, \quad d_i = \frac{1}{i!} \sum_{j=1}^{m} w_j S(t_j) e^{-p_0 t_j} (-t_j)^i, \tag{6}$$

where the coefficients d_i can be calculated easily. Now we come to the second step of the PL method, namely to the application of Padé approximants. The function $\tilde{S}(p)$ can be approximated by Padé approximants (19, 20, 22)

$$\tilde{S}(p) = [N/M]\tilde{S}(q) + O(q^{N+M+1}), \quad q = p - p_0,$$

$$[N/M]\tilde{S}(q) = \frac{A_N(q)}{B_M(q)} = \frac{\sum_{r=0}^{N} a_r q^r}{\sum_{s=1}^{M} b_s q^s}. \tag{7}$$

The coefficients a_r and b_s are obtainable from Taylor coefficients d_i by algebraic methods (e.g., reference 23). The fact that $\tilde{S}(p)$ is represented (within the error $e_m[p]$) by the rational function $\tilde{f}(p)$ (Eqs. 4 and 5) is then taken into account. It follows that the paradiagonal Padé approximant $[n - 1/n]\tilde{S}(q)$ from Eq. 7 should coincide with $\tilde{f}(p)$ within errors introduced by numerical integration and the signal noise:

$$\sum_{k=1}^{n} \frac{C_k}{p - \mu_k} = [n - 1/n]\tilde{S}(q) + e_m(p) + O(q^{2n}). \tag{8}$$

For $e_m(p) \equiv 0$, $O(q^{2n})$ should be identically zero and the roots β'_k, $k = 1, \ldots, n$ of the denominator $B_n(q)$ of $[n - 1/n]\tilde{S}(p)$ correspond to $\mu_k - p_0$. Indeed, $[n - 1/n]\tilde{S}(p)$ can be rewritten as

$$\begin{aligned}
[n - 1/n]\tilde{S}(q) &= \frac{a_{n-1} \prod_{r=1}^{n-1} (q - \gamma'_r)}{b_n \prod_{s=1}^{n} (q - \beta'_s)} \\
&= \frac{a_{n-1} \prod_{r=1}^{n-1} (p - \gamma_r)}{b_n \prod_{s=1}^{n} (p - \beta_s)} \\
&= \sum_{k=1}^{n} \frac{D_k}{p - \beta_k}, \quad \beta_k = \beta'_k + p_0, \\
&\quad \gamma_k = \gamma'_k + p_0,
\end{aligned} \tag{9}$$

where

$$D_k = \frac{a_{n-1} \prod_{r=1}^{n-1} (\beta_k - \gamma_r)}{b_n \prod_{s=1,(s \neq k)}^{n} (\beta_k - \beta_s)} \tag{10}$$

In an ideal situation when $e_m(p) \equiv 0$, β_k are identical to

μ_k and D_k are identical to C_k, $k = 1, \ldots, n$, which formally proves the method.

Determination of the number, n, of components is based on the proven property (20) that paradiagonal Padé approximants $[N - 1/N]f(z)$ for $N > n$ representing the approximant $[n - 1/n]f(z)$, must reduce to $[n - 1/n]f(z)$ through the cancellation of common factors between the numerator and denominator. Thus, by subsequent construction of approximants $[N - 1/N]\tilde{S}(q), N = 1, \ldots, n, n + 1, \ldots$ and determination of their poles and corresponding residues, one should find that for $N \geq n$ actual poles appear regularly in every approximant together with spurious ones. Formally any $[N - 1/N]\tilde{S}(q), N > n$ can be written as

$$[N - 1/N]\tilde{S}(q) = \frac{a_{N-1}\prod_{r=1}^{n-1}(p - \gamma_r)\prod_{r=n}^{N-1}(p - \gamma_r)}{b_N\prod_{s=1}^{n}(p - \beta_s)\prod_{s=n+1}^{N}(p - \beta_s)} \quad (11)$$

Spurious (also called artifical) roots $\{\beta_{n+1}, \ldots, \beta_N\}$ are equal to $\{\gamma_n, \ldots, \gamma_{N-1}\}$ causing cancellation, and the second term in the expression

$$[N - 1/N]\tilde{S}(p) = \sum_{k=1}^{n}\frac{D_k}{p - \beta_k} + \sum_{k=n+1}^{N}\frac{D_k}{p - \beta_k}, \quad (12)$$

should vanish, i.e., coefficients D_k for $k = n + 1, \ldots, N$ are identically zero (cf. Eq. 10). In real situations when $e_m(p) \neq 0$, these coefficients may have nonvanishing, though small values. Furthermore, it is observed that the set of actual roots start to appear for some $N' > n$. This may be considered as the effect of the error $e_m(p) + O(q^{2N'})$ which is taken into account by $N' - n$ terms $D_k/(p - \beta_k)$, $k = n + 1, \ldots, N'$. For subsequent paradiagonal Padé approximants, $N = N' + 1, \ldots$ the set of actual roots appear with noticeable stability while artificial roots are unstable (18, 24, 25).

A global examination of the Padé-Laplace approach (see Fig. 1) shows clearly how the method can be generalized. Thus, if the measured signal is represented by a function of the form

$$F(x) = \sum_{k=1}^{n} f_k(x, \mu_k, C_k),$$

and there is a linear transform which, when applied to this

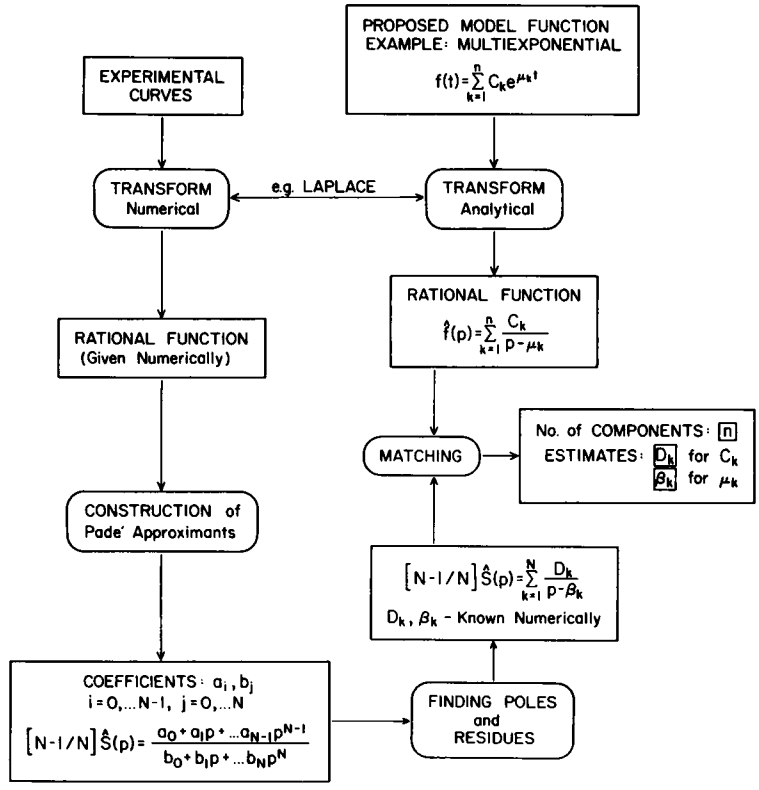

FIGURE 1 Block scheme of the Padé-Laplace method.

function leads to the rational function of the form given in Eq. 4, then we may use the same analysis based on Padé approximants as described above. With this generalization in mind we have investigated the application of the PL method to the analysis of multifrequency phase-modulation fluorometry data.

2.2 Padé-Laplace method in the frequency domain

So far the original PL method has been applied to the analysis of time-dependent signals (18, 25) which can be represented by multiexponential functions. Below we describe how the PL method can be modified for application to signals obtained in the frequency domain which correspond to multiexponential functions in the time domain. We assume that the time and frequency domain are connected as usual by a Fourier transform. In particular we will consider fluorescence intensity decays studied by use of multifrequency phase-modulation fluorometry (7–9).

Assuming that the fluorescence intensity decay is represented by

$$I(t) = \sum_{k=1}^{n} f_k \tau_k^{-1} e^{-t/\tau_k}, \quad \sum_{k=1}^{n} f_k = 1, \quad t \geq 0, \quad \tau_k > 0, \quad (13)$$

where τ_k are the lifetimes and f_k are the corresponding fractions, phase $\phi(\omega)$ and modulation $M(\omega)$ at given frequency ω are (7, 15):

$$\begin{aligned}
\phi(\omega) &= arctg[C(\omega)/S(\omega)], \\
M(\omega) &= [C^2(\omega) + S^2(\omega)]^{1/2} \\
C(\omega) &= M(\omega) \cos \phi(\omega) \\
&= \int_0^\infty I(t) \cos \omega t \, dt = \sum_{k=1}^{n} \frac{f_k}{1 + \omega^2 \tau_k^2}, \\
S(\omega) &= M(\omega) \sin \phi(\omega) \\
&= \int_0^\infty I(t) \sin \omega t \, dt \\
&= \sum_{k=1}^{n} \frac{f_k \omega \tau_k}{1 + \omega^2 \tau_k^2}. \qquad (14)
\end{aligned}$$

Now, we can extend the definition of $I(t)$ to the whole interval $(-\infty, \infty)$ defining $I(t) \equiv 0$ for $t < 0$. Then

$$\begin{aligned}
\mathcal{F}[I](\omega) = M(\omega) e^{i\phi(\omega)} &= \int_{-\infty}^{\infty} I(t) e^{i\omega t} \, dt \\
&= C(\omega) + iS(\omega) \qquad (15)
\end{aligned}$$

is the Fourier transform of $I(t)$. The inverse Fourier transform leads to (see e.g. reference 26):

$$\begin{aligned}
I(t) &= \frac{1}{2\pi} \int_{-\infty}^{\infty} \mathcal{F}[I](\omega) e^{-i\omega t} \, d\omega \\
&= \frac{1}{\pi} \int_{-\infty}^{\infty} d\omega \int_{-\infty}^{\infty} d\tau I(\tau) \cos \omega (\tau - t) \\
&= \frac{1}{\pi} \int_0^\infty d\omega \int_0^\infty d\tau I(\tau) \\
&\quad \cdot [\cos \omega\tau \cos \omega t + \sin \omega\tau \sin \omega t]. \qquad (16)
\end{aligned}$$

Then, by using Eq. 14, we obtain

$$I(t) = \frac{1}{\pi} \int_0^\infty [C(\omega) \cos \omega t + S(\omega) \cos \omega t] \, dt. \qquad (17)$$

To get a rational function of the type shown in Eq. 4 we now apply the Laplace transform to Eq. 17 taking into account Eqs. 13 and 14:

$$\tilde{I}(p) = \mathcal{L}[I](p) = \sum_{k=1}^{n} \frac{f_k \tau_k^{-1}}{p + \tau_k^{-1}} = \frac{1}{\pi} \int_0^\infty \frac{pC(\omega) + \omega S(\omega)}{p^2 + \omega^2}. \qquad (18)$$

We assume that actually measured values of modulation $\bar{M}(\omega_j)$ and phase $\bar{\phi}(\omega_j)$, $j = 1, \ldots, m$ are represented by functions $M(\omega)$ and $\phi(\omega)$:

$$\begin{aligned}
&\bar{M}(\omega_j) = M(\omega_j) + n(\omega_j), \quad \bar{\phi}(\omega_j) = \phi(\omega_j) + \psi(\omega_j), \\
&n(\omega_j) = \sigma(M) n_j, \quad \psi(\omega_j) = \sigma(\phi) \psi_j. \qquad (19)
\end{aligned}$$

Here $n(\omega)$ and $\psi(\omega)$ denote instrumental noise, and $\sigma(M)$ and $\sigma(\phi)$ are standard deviations. In simulations we will use a Gaussian noise so that n_j, ψ_j are considered as normally distributed random numbers centered around zero with unit standard deviation.

The function $\tilde{I}(p)$ can be calculated by numerical integration leading to

$$\begin{aligned}
&\tilde{I}(p) = \tilde{J}(p) + E_m(p), \quad \tilde{J}(p) = \sum_{j=1}^{m} w_j J(\omega_j, p) \\
&J(\omega, p) = \bar{M}(\omega)[p \cos \bar{\phi}(\omega) + \omega \sin \bar{\phi}(\omega)]/(p^2 + \omega^2). \qquad (20)
\end{aligned}$$

Weights w_j and frequencies ω_j should be chosen depending on the numerical integration method used. The error $E_m(p)$ depends on the noise $n(\omega)$ and $\psi(\omega)$ as well as on numerical integration method employed. We can now proceed with analysis by Padé approximants in a completely analogous way to that discussed in the original PL method. Successful recovery of lifetimes and fractions would depend on the error $E_m(p)$ which in principle behaves differently from $e_m(p)$. In fact, it might be expected that $E_m(p)$ is on average greater than $e_m(p)$ due to the difference in the behavior of the integrands in Eqs. 3 and 18 at infinity. By using Eq. 14 it can be shown that the integrand in Eq. 18 behaves like $1/(p^2 + \omega^2)$ as $\omega \to \infty$, while the integrand in Eq. 3 falls off exponentially

when $t \rightarrow \infty$. To reduce $E_m(p)$ we estimated the behavior of the integrand in Eq. 18 for $\omega \rightarrow \infty$ and performed integration from $\omega_{max} \equiv \omega_m$ to infinity analytically. In this paper this portion of the integrand is referred to as the "tail." The details of this procedure are explained in the Appendix.

To construct Padé approximants we need to calculate derivatives of $\tilde{J}(p)$. By applying differentiation rules to $J(\omega, p)$ it is not difficult to derive the following formula for Taylor coefficients d_i:

$$d_i = \frac{(-1)^i}{i!}\frac{d^i}{dp^i}\tilde{J}(p)|_{p=p_0}$$
$$= \sum_{j=1}^{m} w_j'(-1)^i[V_i^C(\omega_j)\bar{C}(\omega_j) + V_i^S(\omega_j)\bar{S}(\omega_j)], \quad i = 1, 2, \ldots \tag{21}$$

$$V_i^C(\omega) = P[p_0 V_{i-1}^C(\omega) - \omega V_{i-1}^S(\omega)],$$
$$V_i^S(\omega) = P[\omega V_{i-1}^C(\omega) + p_0 V_{i-1}^S(\omega)],$$
$$P = (p_0^2 + \omega^2)^{-1}, \quad V_0^C(\omega) = p_0 P, \quad V_0^S(\omega) = \omega P,$$
$$\bar{C}(\omega) = \bar{M}(\omega)\cos\bar{\phi}(\omega), \quad \bar{S}(\omega) = \bar{M}(\omega)\sin\bar{\phi}(\omega).$$

$w_j' = w_j$ for most numerical integration algorithms; the exception is our "generalized trapezoidal rule" (see below and Appendix).

Calculating subsequent paradiagonal Padé approximants, the method as described above should allow recovery of lifetimes τ_k as

$$\tau_k = -1/(q_k + p_0),$$
$$q_k = \text{Real pole of } [N - 1/N]\tilde{J}(p - p_0),$$
$$k = 1, \ldots, \quad n, \quad N \geq n. \tag{22}$$

Corresponding fractions f_k can be calculated from the residues at these poles:

$$Res_{z=q_k}\{[N - 1/N]\tilde{J}(z - p_0)\} = f_k\tau_k^{-1}. \tag{23}$$

It was noted by Yeramian and Claverie (18, 24, 25) that the choice of the numerical integration method can improve the recovery of components. They found that simple trapezoidal and Simpson's rules are good choices for noisy data. We used both rules and in addition a method which we developed specifically for analysis of the phase/modulation data which we have called the "generalized trapezoidal rule" because the interpolation between two subsequent abscissas ω_1 and ω_2 is not linear but for the functions $C(\omega)$ and $S(\omega)$ are given by $c_1/(1 + \omega^2 c_2)$ and $s_1\omega/(1 + \omega^2 s_2)$, respectively. The parameters c_1 and c_2 are easily determined from known values $\bar{C}(\omega_1)$ and $\bar{C}(\omega_2)$ and analogously, s_1 and s_2 from $\bar{S}(\omega_1)$ and $\bar{S}(\omega_2)$. These interpolating functions represent exactly $C(\omega)$ and $S(\omega)$ in the case of one component and zero noise, whereas it may be a good approximation when one component is dominant (for details see Appendix). We have also considered a fitting procedure for $\bar{C}(\omega)$ and $\bar{S}(\omega)$ which employs cubic splines and then integration to the required accuracy. Although intuitively appealing, in actual examples this method did not show any particular advantages. The best results were obtained by using either a simple trapezoidal rule or the generalized trapezoial rule. In the latter case we found it convenient to change the integration variable ω according to the transformation: $\omega = \omega_0(1 - x)/x$, which leads to the change of integration limits from $[0, \infty]$ to $[0, 1]$.

The only input parameter for the PL method is p_0. Theoretically, the PL method should work for any p_0, but numerical calculations have shown that the optimal choice of p_0 is the one which leads to Taylor coefficients d_i of the same order of magnitude (24). This can be achieved if we require that $d_{i+1}/d_i \rightarrow 1$ when $i \rightarrow \infty$ (24). It may be shown that if the only singularity on the circumference of the circle of convergence of the Taylor series

$$\sum_{i=0}^{\infty} d_i(p - p_0)^i$$

is at pole $p = \mu$, then $d_i/d_{i+1} \rightarrow \mu - p_0$ when $i \rightarrow \infty$. Thus we may adopt the following procedure for searching $p_{0,optimal} > 0$ (24): starting from $p_{0,initial} > 0$ we calculate the corresponding Taylor coefficients d_i and then $p_{0,optimal}$ is given by

$$p_{0,optimal} = \lim_{i\rightarrow\infty}(d_i/d_{i+1}) + p_{0,initial} + 1. \tag{24}$$

This means that $p_{0,optimal}$ is at a distance equal to 1 from the largest (negative) pole which in our case corresponds to the longest lifetime.

3. RESULTS AND DISCUSSION

3.1 Simulations

The original PL method has been tested on simulated data with excellent results (e.g., Table 5 of reference 25 shows comparison with other methods for multiexponential analysis; see also references 18 and 24). Here we tested the modified Padé-Laplace (MPL) method under specific conditions of phase/modulation measurements.

The simulations were chosen to show the effectiveness and limits of the method. The crucial limitation in recovery of components comes from the level of noise in the data. Unless otherwise stated we chose to use Gaussian noise with a standard deviation $\sigma(M) = 0.005$ in modulation and $\sigma(\phi) = 0.2°$ in phase, the typical level of noise in phase/modulation measurements performed in our laboratory. However, we have observed that it is

possible to perform measurements with average standard deviations $\bar{\sigma}(M) \leq 0.001$ and $\bar{\sigma}(\phi) \leq 0.04°$ (e.g., see measurements on phospholipase A_2, section 3.2). To investigate the limits of the method in the most favorable case we also chose Gaussian noise with standard deviations $\sigma(M) = 0.001$ and $\sigma(\phi) = 0.04°$. The data simulated with this level of noise will be referred to as low noise data. Other constraints which are met in actual phase/modulation measurements deal with minimal and maximal frequency. In simulated data we choose the minimal circular frequency as $\omega_{min} = 2\pi\nu_{min}$, $\nu_{min} \leq 4$ MHz and maximal circular frequency $\omega_{max} = 2\pi\nu_{max}$, such that $\phi(\omega_{max}) < 80°$.

As a first example we applied the MPL method to a simulated decay with two exponential components (Table 1), and on this example we will explain the features of the method important for its practical use. For the numerical integration we used the simple trapezoidal rule (unless otherwise stated) and tail estimation as described in Appendix. In Table 1 we have shown only the meaningful recovered lifetimes and fractions, those which correspond to the poles and residues with a negligible or zero imaginary part. It is clear that more or less accurate recovery of two genuine components starts at a Padé approximant of the order [3/4] and appears repeatedly up to order [18/19]. The exceptions are Padé approximants of orders [5/6] and [7/8], where a spurious low fraction component appears. Theoretically the recovery of two genuine components should start at Padé approximant of order [1/2], but as already mentioned (18, 25) this is not the case due to the inaccuracy of the numerical integration and noise in the data. In fact, even for the noiselss data in this example, we found that Padé approximant [3/4] is the first to recover genuine components, which are then accurately (to three or more significant digits) recovered in all Padé approximants up to the order [19/20]. The accuracy of a given recovery can be estimated by a single number which we will call the total relative error (TRE), defined as:

$$\mathrm{TRE} = \sum_{k=1}^{n} \left| \frac{\tau - \tau_k^R}{\tau_k} \right| + \left| \frac{f_k - f_k^R}{f_k} \right|. \qquad (25)$$

Here τ_k and f_k are exact, and τ_k^R and f_k^R are recovered values for lifetimes and fractions, respectively. Obviously, TRE can be used to determine how close recovered values are to exact ones only in simulations for which the latter are known. However, this quantity is also useful for judging the quality of the tests used to assess the recoveries from real data. We investigated several such tests, combining functions $C(\omega)$ and $S(\omega)$ as given by recovered lifetimes and fractions and by data (cf. Eqs. 14 and 21). The most useful we found was the standard reduced

TABLE 1 Two-component simulation

[N/N − 1]	τ_k^R	f_k^R	R	χ_r^2	TRE
[1/2]	1.6336	0.82632			
	0.14571	0.02797	0.3293	83.15	2.277
[2/3]	6.0938	0.23103			
	1.1169	0.78799	0.01902	20.67	0.960
[3/4]	3.8182	0.32476			
	0.9350	0.70497	0.02973	35.50	0.200
[4/5]	3.8113	0.32555			
	0.9331	0.70485	0.03041	37.44	0.206
[5/6]	3.9676	0.29093			
	2.0206	0.07640			
	0.8880	0.67442	0.04175	76.00	
[6/7]	3.8145	0.32455			
	0.9391	0.70104	0.02559	28.21	0.191
[7/8]	8.7143	0.04102			
	1.0580	0.75706	0.20192	228.15	2.181
[8/9]	3.8105	0.32818			
	0.8963	0.76563	0.09381	215.36	0.339
[9/10]	3.7846	0.33100			
	0.8750	0.80546	0.13646	415.42	0.433
[10/11]	3.9816	0.30620			
	0.9780	0.71076	0.01696	8.10	0.063
[11/12]	3.8090	0.34767			
	1.0454	0.80861	0.15629	206.22	0.407
[12/13]	3.8091	0.34733			
	1.0455	0.80883	0.15616	206.19	0.406
[13/14]	3.7664	0.36342			
	1.0351	0.77734	0.14076	156.11	0.415
[14/15]	4.0400	0.30144			
	0.9854	0.71357	0.01501	6.03	0.049
[15/16]	4.0525	0.30013			
	0.9886	0.71321	0.01335	4.77	0.044
[16/17]	4.6818	0.36018			
	1.0264	0.72428	0.08445	28.63	0.432
[17/18]	3.9686	0.31790			
	0.9827	0.70285	0.02074	4.48	0.089
[18/19]	3.9685	0.31802			
	0.9827	0.71496	0.03298	10.96	0.107
[19/20]	1.4526	0.43853			
	4.4868	0.22039			
	0.6085	0.44241	0.10133	539.15	
[A16]	4.07 ± 0.19	0.302 ± 0.006			
	1.00 ± 0.01	0.701 ± 0.018		1.02	0.027
[A32]	4.05 ± 0.17	0.302 ± 0.007			
	1.00 ± 0.01	0.700 ± 0.017		1.03	0.022
[LMfit]	3.99 ± 0.07	0.301 ± 0.004			
	0.999 ± 0.004	0.699 ± 0.004		1.01	0.009
[A16]	3.93 ± 0.03	0.309 ± 0.005			
(200)	1.001 ± 0.008	0.688 ± 0.005		2.11	0.064
[LMfit]	3.99 ± 0.09	0.302 ± 0.007			
(200)	0.997 ± 0.008	0.698 ± 0.007		1.07	0.015

Exact lifetimes: $\tau_1 = 4$ ns, $\tau_2 = 1$ ns; exact fractions: $f_1 = 0.3$ $f_2 = 0.7$. 50 phase/molulation data, equally spaced in frequency were simulated; maximal frequency, = 300 MHz; minimal frequency, 6 MHz. $\sigma(M) = 0.005$, $\sigma(\phi) = 0.2°$; $p_0 = 0.8$ ns^{-1}. [A16] and [A32] stand for averages over recoveries with minimal χ_r^2 for 16 and 32 different p_0, respectively (see text). Two last results marked by (200) correspond to 20 phase/modulation data, equally spaced in x-variable (see text) with maximal frequency of 200 MHz, minimal frequency of 4.1 MHz and minimal difference between two subsequent frequencies of 4.1 MHz.

chi-squared:

$$\chi_\nu^2 = \nu^{-1} \sum_{j=1}^{m} \frac{[\bar{M}(\omega_j) - M_R(\omega_j)]^2}{\sigma_j^2(M)} + \frac{[\bar{\phi}(\omega_j) - \phi_R(\omega_j)]^2}{\sigma_j^2(\phi)}, \quad \nu = m - n_R + 1. \quad (26)$$

Here $M_R(\omega_j)$ and $\phi_R(\omega_j)$ are modulation and phase, respectively, given by recovered lifetimes τ_k^R, fractions f_k^R and number of components n_R (see Eq. 14). $\sigma_j(M), j = 1, \ldots, m$ denote standard deviations in modulation and $\sigma_j(\phi)$ denote standard deviation in phase. Another useful test for the quality of recovery is the quantity

$$R = \left| 1 - \sum_{k=1}^{n_R} f_k^R \right|, \quad (27)$$

which, according to Eq. 13, should be equal to zero. Table 1 reveals that both χ_ν^2 and R are reasonably well correlated with TRE, and this we found to be true in many other examples. However, occasionally a lower χ_ν^2 may correspond to a higher TRE as one can see by comparing recoveries [17/18] and [14/15]. In another simulation ($\tau_1 = 4$ ns, $\tau_2 = 2$ ns, $f_1 = 0.4, f_2 = 0.6$), this effect is much more emphasized: Comparing two recoveries, we found that $\chi_\nu^2 = 1.18$ corresponds to TRE = 0.58 while $\chi_\nu^2 = 14.4$ corresponds to TRE = 0.09 and when the same data were fitted by a standard least-square technique an almost ideal $\chi_\nu^2 = 1.01$ corresponds to TRE = 0.19. This phenomenon arises from the statistical nature of χ_ν^2 which, when minimized, yields parameters which are most probably, but not inevitably, closest to the true values. For sake of comparison, in all presented simulations we add also the recovery of parameters obtained by standard least-square fitting via the Levenberg-Marquardt (LM) algorithm as implemented in reference (27).

The recovery with the lowest TRE in the example shown in Table 1 corresponds to the minimal R obtained. This is not always the case, but by imposing an upper limit to the acceptable R we can eliminate most of those recoveries which are not close to genuine lifetimes and fractions. Thus, by imposing the condition that $R < 0.05$ we can eliminate all recoveries with TRE > 0.21 (with the only exceptions being recoveries [1/2] and [2/3]). We found it useful to display all recoveries for which $R < 0.05$ in two-dimensional scattergrams which show clustering of recovered lifetime-fraction points around their exact positions (Fig. 2). In this way one can easily delineate spurious recoveries (such as the low-fraction component in [5/6]) and get a feeling for the distribution of lifetimes and fractions clustered around the best possible recovery. Such a graphical aid is especially valuable when the sequence of relatively accurate recoveries does not appear regularly in subsequent Padé approximants. The irregularities occur as a consequence of noise in the data, and errors in the numerical integration.

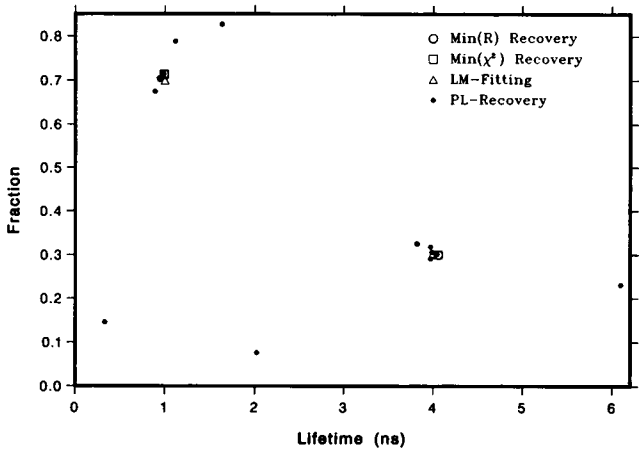

FIGURE 2 The lifetime-fraction scattergram for a two-component simulation *a* of Table 1.

According to the procedure of the original PL method (18, 24), when a certain set of poles and corresponding residues appear repeatedly in subsequent Padé approximants with negligible variation in values, it is considered to represent the recovery of the parameters of underlying multiexponential function. In the example displayed in Table 1 we find that the recovery [3/4]: $\tau_1^R = 3.818$ ns, $\tau_2^R = 0.935$ ns, $f_1^R = 0.325, f_2^R = 0.705$ is repeated in Padé approximants [4/5] and [6/7] with fair accuracy. However, when the ratio of exact lifetimes is smaller (~1.5) such regular behavior disappears. Therefore, based on empirical evidence from many simulations we propose another procedure: As the best estimate of lifetimes and fractions one chooses the average values of lifetimes and corresponding fractions obtained from the recovery with minimal R and the recovery with minimal χ_ν^2 when 20 subsequent Padé approximants are evaluated. In the example considered we obtain $\tau_1^R = 4.0106$ ns, $\tau_2^R = 0.9856$ ns, $f_1^R = 0.3090, f_2^R = 0.7080$ with TRE = 0.059, which is considerably smaller than TRE for the recovery [3/4]. Often the recovery with minimal χ_ν^2 is also the recovery with minimal R.

In the original PL method no procedure was described to estimate the uncertainties in recovered parameters. Here we propose a procedure based on variation of the parameter p_0. As we already pointed out, theoretically the PL method should work for any p_0 for which a Laplace transform exists. However, due to the noise in the data and errors in numerical integration there is an optimal choice of p_0 given by Eq. 24. By varying p_0 around $p_{0,\text{optimal}}$ we can obtain different sets of recoveries each correspond-

ing to a given p_0. Within a given set of recoveries, we choose as the "best" recovery the one corresponding to minimal χ^2_r. The set of these "best" recoveries for all p_0 considered form a set from which we determine the uncertainty in recovered lifetimes and fractions as well as their best estimates. Sometimes the set of "best" recoveries may contain a few recoveries with evidently spurious components. After removing such recoveries we take the averages of the rest of the mutually corresponding lifetimes and fractions and consider them as the best estimates. We found by simulation that minimal χ^2_r lifetimes and fractions for 256 randomly chosen p_0 (normally distributed around $p_{0,\text{optimal}}$) do not follow a Gaussian distribution. Therefore, we estimated the uncertainties on the basis of Chebyshev's inequality (28) which states that the proportion of numbers in a population which deviate from the population mean by at least $k\sigma$ is less than or equal to $1/k^2$, where σ is the standard deviation. We calculate the standard deviation by use of the above obtained averages of lifetimes and corresponding fractions as population means. The uncertainty in lifetimes and fractions is then given by corresponding standard deviation multiplied by k. We found empirically that $k = \sqrt{2}$ (corresponding to a proportion of 50%) gives satisfactory results. In Table 1 we show the results for 16 and 32 randomly chosen p_0 values normally distributed around $p_{0,\text{optimal}} = 0.8\ \text{ns}^{-1}$. (In the case of 16 "best" recoveries one contained a spurious component and was removed; in case of 32, two were removed.) The results are equivalent and estimated lifetimes and fractions are closer to the true values than those obtained by averaging recoveries for minimal χ^2_r and minimal R. As a rule of thumb we have chosen to use 16 randomly chosen p_0 distributed normally with $p_{0,\text{optimal}}$ as a mean (usually $<1\ \text{ns}^{-1}$) and with a standard deviation of $0.01\ \text{ns}^{-1}$.

A few remarks are warranted regarding the determination of $p_{0,\text{optimal}}$. In Fig. 3 we show the typical behavior of p_i defined as

$$p_i = d_i/d_{i+1} + p_{0,\text{initial}} + 1, \quad i = 1,2,\ldots \tag{28}$$

with and without noise in the simulated data. According to Eq. 24 $p_{0,\text{optimal}} = \lim_{i\to\infty} p_i$ and in the case of noiseless data the limit is readily obtained. For noisy data, the limiting value is usually less obvious. In such circumstances we estimate $p_{0,\text{optimal}}$ taking the average $(p_{m-1} + p_m + p_{m+1})/3$, where p_m denotes the first maximum (or minimum) value of p_i characterized by slow change of p_i for $i < m$ and faster change for $i > m$.

In simulation *a* shown in Table 1, we have chosen phase/modulation data at 50 equidistant frequencies with $\nu_{\max} = 300$ MHz. The precision of phase modulation measurements is sometimes decreased at higher frequencies. Therefore in simulation *b* of Table 1 we choose

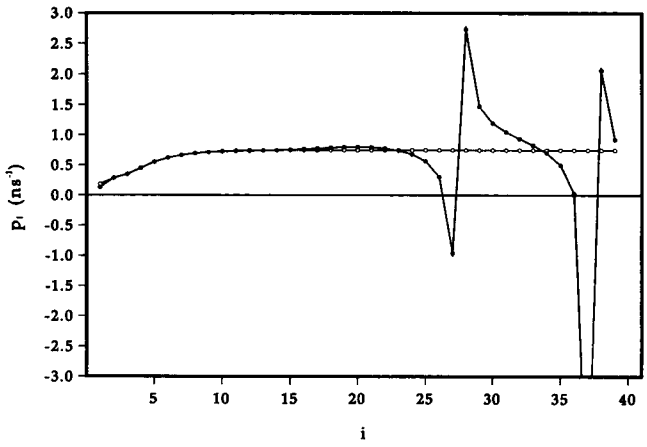

FIGURE 3 The behavior of p_i as defined by Eq. 28 for the simulation *a* of Table 1 with (●) and without (○) noise.

$\nu_{\max} = 200$ MHz. In this case we used the generalized trapezoidal integration (described in section 2.1 and in Appendix). We found this to be more efficient than simple trapezoidal integration when the maximal frequencies are lower and when less data are available. The integration is conveniently performed by change of integration variable ω to $x = \omega_0/(\omega + \omega_0)$, where ω_0 is uniquely determined by requiring an equidistant distribution of data in x-variable, fixed $\nu_{\min}$, number of data, and a minimal difference between two subsequent frequencies. Although in simulation *b* of Table 1 we sampled only 20 phase/modulation data pairs, parameter recovery by the MPL method is good.

In the next examples we investigate the limits of the MPL method. For a given level of noise two components can still be resolved for some critical ratio $(\tau_1/\tau_2)_{\text{crit}}$. Two simulations in Table 2 with lifetimes ratio $\tau_1/\tau_2 = 1.5$ are identical except for different realizations of the noise in the data (different sets of random numbers n_j, ψ_j; cf. Eq. 19). The quality of recovery from both the MPL method and standard LM-fitting clearly depends on the noise in the data. These simulations show how both methods might give either good or poor results when the lifetime ratio is close to $(\tau_1/\tau_2)_{\text{crit}}$. In Fig. 4 we show the phase/modulation data and the theoretical curves obtained for recoveries (2) and (3) from Table 2. Although the curve for recovery (2) does not fit the data as well as the curve for recovery (3), the lifetimes and the fractions corresponding to recovery (2) are much closer to the true values. This clearly shows the usefulness of the MPL method which is directed towards the recovery of the parameters regardless of the apparent "fits" to the data profile.

By performing a series of simulations with $f_1 = f_2 = 0.5$,

TABLE 2 **Two-component simulations with close lifetimes or small fractions**

	τ_1	τ_2	f_1	f_2	TRE	χ^2_r
	ns	*ns*				
(1) Exact	3	2	0.4	0.6		
(2) MPL	2.96 ± 0.07	2.03 ± 0.10	0.43 ± 0.10	0.56 ± 0.05	0.17	4.27
(3) LM-fit	2.76 ± 0.13	1.84 ± 0.10	0.60 ± 0.12	0.40 ± 0.12	0.99	0.85
(4) MPL	3.35 ± 0.22	2.10 ± 0.06	0.24 ± 0.10	0.76 ± 0.10	0.83	0.96
(5) LM-fit	3.02 ± 0.20	1.97 ± 0.07	0.42 ± 0.11	0.58 ± 0.11	0.09	0.98
(6) Exact	3	2.6	0.5	0.5		
(7) MPL	2.98 ± 0.09	2.59 ± 0.15	0.53 ± 0.34	0.47 ± 0.34	0.13	1.72
(8) LM-fit	3.72 ± 0.21	2.73 ± 0.01	0.07 ± 0.02	0.93 ± 0.02	2.00	0.94
(9) LM-fit	3.06 ± 0.08	2.63 ± 0.05	0.38 ± 0.14	0.62 ± 0.14	0.51	0.97
(10) Exact	3	1	0.05	0.95		
(11) MPL	3.01 ± 0.31	1.007 ± 0.014	0.050 ± 0.010	0.955 ± 0.010	0.02	1.51
(12) LM-fit	3.01 ± 0.40	0.999 ± 0.005	0.051 ± 0.009	0.969 ± 0.009	0.03	1.01

(1) Phase/modulation data with these lifetimes and fractions simulated as in Table 1 *a*; noise realization A. (2) The result of analysis of data (1) by MPL-method using 16 different p_0 values (see text). (3) The result of analysis of data (1) by use of least-square fitting (Levenberg-Marquardt algorithm). (4) and (5) The same as in (2) and (3), respectively, with noise realization B. (6) Phase/modulation data with these lifetimes and fractions simulated as in Table 1 *a*, adding low noise $\sigma(M) = 0.001, \sigma(\phi) = 0.64°$. (7) The result of analysis of data (6) by MPL-method as in (2). (8) The result of analysis of data (6) as in (3) with an initial guess $\tau_1 = 4$ ns, $\tau_2 = 2$ ns, $f_1 = 0.4$. (9) The result of analysis as in (8) with an initial guess $\tau_1 = 2.9$ ns, $\tau_2 = 2.5$ ns, $f_1 = 0.51$. (10) Phase/modulation data with these lifetimes and fractions are simulated as in Table 1 *a*. (11) The result of analysis of data (10) as in (2). (12) The result of analyses of data (10) as in (3).

$\tau_1 = 3$ ns and τ_2 varied, we estimated the critical lifetime ratio for a given level of noise, as 1.4. The next example in Table 2 corresponds to a simulation with low noise data. It is an example of the series of simulations with $f_1 = f_2 = 0.5$, $\tau_1 = 3$ ns and τ_2 varied between 2.5 ns and 2.8 ns. As can be seen when $\tau_2 = 2.6$ ns two components are still resolved; the critical lifetime ratio for this level of noise is estimated to be 1.15. Note that the standard method is very sensitive to the initial guess in this case. The last example of Table 2 illustrates the ability of the MPL method to recover components with small fractions ($f_1 = 0.05$). The ratio of amplitudes (preexponential factors) in this case is as much as 57. The method failed to recover small fraction components when this ratio was 100.

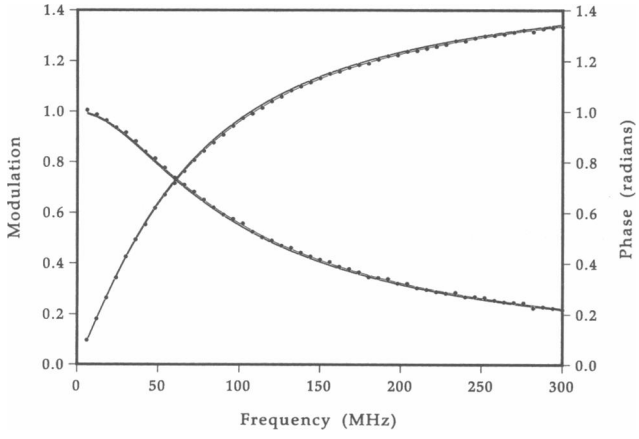

FIGURE 4 Phase/modulation data for simulation *1* of Table 2 and theoretical curves obtained for MPL recovery 2 (*thick line*) and for LM-fit recovery 3 (*thin line*).

In the case of a three component simulation the MPL and standard methods can resolve components with ratios of lifetimes $\tau_1/\tau_2 \approx \tau_2/\tau_3 \geq 2.4$ at a given noise level. In the example (2) shown in Table 3 the MPL method was more successful than the standard method, but for other realizations of the noise in the data both methods gave similar results. The next three component simulation (Table 3) corresponds to real data analysis of the phase/modulation data on tryptophan fluorescence from phospholipase A_2 (see section 3.2). Only 16 phase/modulation data pairs with low noise were simulated. By use of the MPL method with the generalized trapezoidal rule integration, we obtained satisfactory results. The standard method in this case provided a result with remarkably low TRE. We also applied the MPL method to a four-component simulation. A reasonable recovery is obtained for low noise data (Table 3, section 3) by both MPL and standard methods.

Our final example deals with the important question of lifetime distributions. We simulated phase/modulation data assuming that the lifetimes are distributed according to a bimodal Lorentzian distribution (15) with centers at 1.37 ns and 4.33 ns. Results of the analysis by the MPL method and LM-fitting to the three components are displayed on Fig. 5 (the details of simulation and analysis are given in the figure legend). In only one of the Padé approximants of the orders [2/3], [3/4], . . . , [18/19]

TABLE 3 Three- and four-component simulations

		Exact	MPL	LM-fit
(1)	$\tau_1(ns)$	5	5.18 ± 0.09	6.44 ± 0.69
	$\tau_2(ns)$	2.3	2.42 ± 0.32	2.82 ± 0.21
	$\tau_3(ns)$	1	1.03 ± 0.11	1.02 ± 0.02
	f_1	0.333	0.31 ± 0.03	0.18 ± 0.05
	f_2	0.333	0.33 ± 0.07	0.45 ± 0.04
	f_3	0.334	0.35 ± 0.10	0.36 ± 0.06
			TRE = 0.26 χ^2_r = 1.12	TRE = 1.44 χ^2_r = 0.97
(2)	$\tau_1(ns)$	6	5.97 ± 0.07	6.01 ± 0.07
	$\tau_2(ns)$	2	2.00 ± 0.02	2.00 ± 0.03
	$\tau_3(ns)$	0.5	0.47 ± 0.01	0.50 ± 0.01
	f_1	0.3	0.302 ± 0.005	0.300 ± 0.006
	f_2	0.5	0.502 ± 0.004	0.500 ± 0.003
	f_3	0.2	0.197 ± 0.003	0.200 ± 0.007
			TRE = 0.09 χ^2_r = 10.15	TRE = 0.007 χ^2_r = 1.13
(3)	$\tau_1(ns)$	11	10.82 ± 0.65	10.80 ± 0.12
	$\tau_2(ns)$	3.5	3.42 ± 0.53	3.40 ± 0.07
	$\tau_3(ns)$	1	1.01 ± 0.07	0.998 ± 0.006
	$\tau_4(ns)$	0.2	0.20 ± 0.05	0.2002± 0.008
	f_1	0.2	0.20 ± 0.03	0.207 ± 0.0004
	f_2	0.2	0.198 ± 0.005	0.195 ± 0.002
	f_3	0.4	0.392 ± 0.005	0.398 ± 0.002
	f_4	0.2	0.21 ± 0.02	0.200 ± 0.005
			TRE = 0.17 χ^2_r = 172.5	TRE = 0.13 χ^2_r = 0.92

(1) Phase/modulation data with this exact lifetime and fractions simulated as in Table 1 *a*. The results are from the analysis by MPL-method using 16 different p_0 values (see text) and by least-square method. (2) 16 phase/modulation data, equally spaced in *x*-variable (see text) were simulated; maximal frequency, 190 MHz; minimal frequency, 20 MHz; minimal difference between two subsequent frequencies, 4 MHz. $\sigma(M) = 0.001$, $\sigma(\phi) = 0.04°$. (3) 100 phase/modulation data, equally spaced in frequency were simulated; maximal frequency, 500 MHz; minimal frequency, 5MHz; noise level as in (2).

were two components recovered; all others led to three or four components. Fig. 5 shows that MPL recoveries are more dispersed than clustered indicating that there are no well-defined exponential components. The scattergram of MPL recoveries may thus serve as a test of whether phase/modulation data can be better described by continuous lifetime distributions or by discrete lifetimes.

3.2 Tests on real data

Now we present examples in which we have applied the modified Padé-Laplace method to the analysis of measured phase/modulation data. Fluorescence lifetimes were measured by multifrequency phase fluorometry (7–9). The fluorometer used is similar to that described earlier (29), but employed a synchronously pumped and mode-locked Nd:YAG laser (Spectra-Physics Inc., Mountain View, CA) as the primary light source (Sedarous, S. S., J. M. Francois, J. R. Alcala, C. Gerday, E. Gratton, and F. G. Prendergast, manuscript in preparation). The frequency doubled output from the laser was used to pump a dye laser (rhodamine 6G) and the output from the dye laser was frequency doubled to yield excitation light in the wavelength range 285–315 nm. For excitation wavelengths >315 nm the excitation source was an Argon ion laser (Spectra-Physics 2025) with ultraviolet excitation at 351 and 363 nm. In this latter instance a Pockels cell was used to effect amplitude modulation of the exciting light. All samples were temperature controlled (at 25°). Fluorescence was collected through appropriate cut-off or interference filters to eliminate Rayleigh and Raman scattering and detected by use of model R928 phototubes (Hamamatsu Phototonics K.K., Hamamatsu City, Japan). Cross correlation techniques afforded measurement of phase angles and relative demodulation. All fluorophores were of laser grade purity. Purified porcine pancreatic phospholipase A_2 was the kind gift of Dr. S. Hendrickson, St. Olaf College, Northfield, MN.

Our first example is the fluorescence decay of 2.5 μM anthracene in cyclohexane (Fig. 6). The scattergram clearly shows one component and the values recovered agree well with those obtained by standard procedures. (More details of the analysis are given in the figure

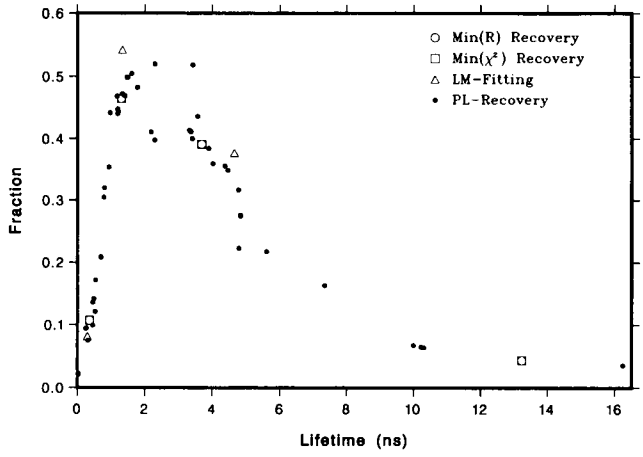

FIGURE 5 The lifetime-fraction scattergram for the simulation with bimodal Lorentzian lifetime distribution. The distribution is constructed using parameters from reference 15, Table 3 for PLA2; center 1, 1.37 ns; width 1, 1.21 ns; fraction, 0.47; center 2, 4.33 ns; width 2, 0.38 ns. The Gaussian noise with $\sigma(M) = 0.001$ and $\sigma(\phi) = 0.05°$ is added to 50 phase/modulation data (equally spaced in frequency) generated by assuming the lifetime distribution. PL recoveries are obtained with $p_0 = 0.9$ ns^{-1}. Number of Padé approximants: 19, 15 satisfying $R < 0.05$. Assuming three-component decay, LM least-square fit to these data was performed with several initial guesses which all led to the result displayed ($\chi^2_\nu = 8.4$).

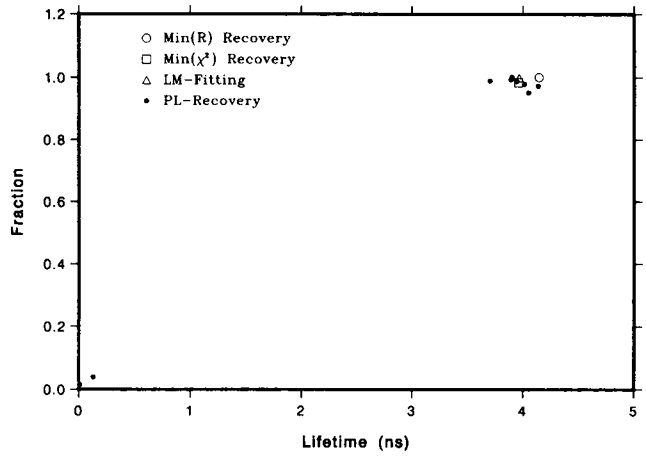

FIGURE 6 The lifetime-fraction scattergram for 2.5 μM anthracene in cyclohexane at 25C°. Excitation: 351 nm. Emission: KV-418. 42 phase/modulation data points were collected. Minimal frequency: 4.9 MHz. Maximal frequency: 180 MHz. Method of integration: trapezoidal rule. $p_0 = 0.75$ ns^{-1}. Number of Padé approximants: 15, 11 satisfying $R < 0.05$.

Recovery	n	τ_k	f_k	χ^2_ν	R
Min (R)	1	4.145	1.001	2587.7	0.001
Min (χ^2)	1	3.962	0.985	132.0	0.149
Average	1	4.056	0.993	772.7	0.007
Average (16)	1	3.962 ± 0.004	0.985 ± 0.001	132.1	0.149
LM-fit	1	3.966 ± 0.0004	1	152.9	0
ISS-fit*	1	4.126 ± 0.039	1	116.4	0

*Only 18 modulation/phase data points were taken into account.

legend.) The parameter p_0 was chosen to be 0.75 ns, and this value was recovered as $p_{0,\text{optimal}}$ according to Eq. 24. (χ^2_ν values are high because we didn't attempt to remove "outliers" in phase/modulation data points.) In this and the following examples we display the recoveries corresponding to minimal R and minimal χ^2_ν, their average, and the average of 16 recoveries for different p_0 as described in section 3.1. In addition we show the analysis performed by least-square fitting using Levenberg-Marquardt algorithm and the analysis performed by standard ISS/Sperry Univac (Santa Clara, CA) software (which, however, was set up to use maximally 25 phase/modulation data points).

In Fig. 7, *a* and *b*, we show the results of the analysis for the fluorescence decay of 5 μM *p*-terphenyl in cyclohexane; for this example we analyzed only 18 phase/modulation data points. The scattergrams show that the recoveries obtained by use of the generalized trapezoidal rule with change of integration variable (Fig. 7 *b*) are more consistent than the recoveries obtained by use of the trapezoidal rule (Fig. 7 *a*). We observed that when there is a smaller number of phase/modulation data points (<40), the application of the generalized trapezoidal rule with change of integration variable gives more consistent recoveries. The same is true when the maximal frequency at which phase and modulation ratio have been measured is relatively low (<200 MHz). In this example all methods gave very similar results. In Fig. 8 we show the results of the analysis for fluorescence decay of the mixture: 1.25 μM Dim 1,4-bis-2-(4-methyl-5-phenyloxazolyl)-benzene (POPOP) and 4.9 μM 1,6-diphenylhexatriene in ethanol. The scattergram clearly shows two components; recovery with minimal R coincides with recovery with minimal χ^2_ν. The parameter p_0 was initially chosen to be 0.8 ns^{-1} and the value 0.708 ns^{-1} returned as optimal was used to obtain the result with averaging over 16 recoveries. In this example all methods gave results consistent within uncertainties of the MPL method and standard least-squares fit (ISS).

Our last example is the analysis of 10 μM phospholipase A_2 in 20 mM 3-(*N*-morpholino) propane sulfonic acid (MOPS) (Fig. 9). Three components are recovered in good agreement with results from standard methods. The curves obtained from MPL average (16) recovery (Fig. 9 *b*) deviate somewhat from the data points, but according to illustration given in Fig. 4 this does not automatically mean that recovered lifetimes and fractions are not close to the "true" ones. It is worth noticing that in this example only 16 phase/modulation data pairs with a maximal frequency of 189 MHz were available, and

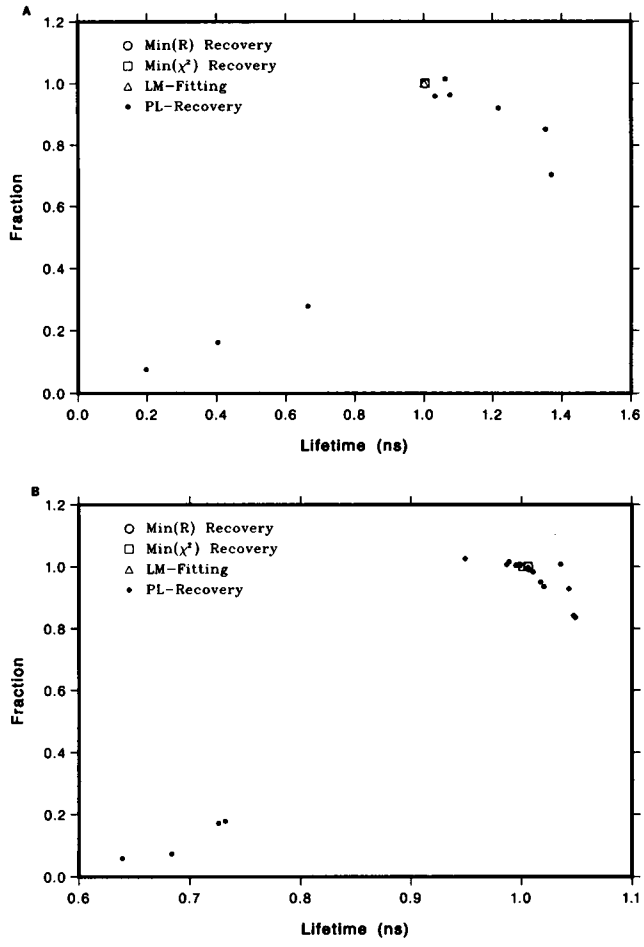

FIGURE 7 (*a*) The lifetime-fraction scattergram for 5 μM *p*-terphenyl in cyclohexane at 23C°. Excitation 295 nm. Emission: WG-320. 18 phase/modulation data points were collected. Minimal frequency: 8.21 MHz; Maximal frequency: 303.67 MHz. Method of integration: trapezoidal rule. $p_0 = 1$ ns^{-1}. Number of Padé approximants: 20, 8 satisfying $R < 0.05$. (*b*) The lifetime-fraction scattergram for the data give in *a*. Method of integration: generalized trapezoidal rule. $p_0 = 1$ ns^{-1}. Number of Padé approximants: 20, 18 satisfying $R < 0.05$.

	n	τ_k	f_k	χ^2_r	R
Recovery *a*					
Min (*R*)	1	1.0033	1.0004	0.00002*	0.0004
Min (χ^2)	Coincides with Min (*R*)				
Average (16)	1	1.0033 ± 0.0009	1.0004 ± 0.0001	0.00002*	0.0004
LM-fit		1.00062 ± 0.00001	1	0.00002*	0
ISS-fit	1	1.004 ± 0.002	1	0.633	0
Recovery *b*					
Min (*R*)	1	1.006	1.009	0.00002*	0.0009
Min (χ^2)	Coincides with Min (*R*)				
Average (16)	1	1.003 ± 0.004	1.001 ± 0.001	0.00002*	0.001

*χ^2 was not weighted, but the phase and the modulation are comensurable because the phase is expressed in radians.

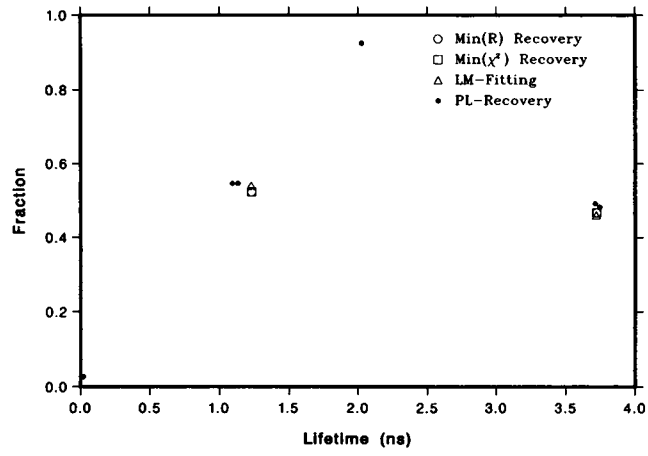

FIGURE 8 The lifetime-fraction scattergram for a mixture of 1.25 μM Dim POPOP and 4.9 μM 1,6-diphenylhexatriene in ethanol. Excitation: 351 nm. Emission: KV-418. 50 phase/modulation data points were collected. Minimal frequency, 4.9 MHz; maximal frequency, 200 MHz trapezoidal rule. $p_0 = 0.8$ ns^{-1}. Number of Padé approximants: 20, 4 satisfying $R < 0.05$.

Recovery	n	τ_k	f_k	χ^2_r	R
Min (*R*)	1	3.723	0.467		
	2	1.231	0.523	90.8	0.01
Min (χ^2)	Coincides with Min (*R*) recovery				
Average (16)	1	4.02 ± 0.68	0.45 ± 0.05		
	2	1.24 ± 0.08	0.58 ± 0.08	188.5	0.03
LM-fit	1	3.719 ± 0.008	0.460 ± 0.001		
	2	1.228 ± 0.001	0.539 ± 0.001	22.5	0
ISS-fit*	1	3.8 ± 0.3	0.51 ± 0.04		
	2	1.18 ± 0.05	0.49	4.4	0

*Only 15 modulation/phase data points were taken into account.

application of the PL method with simple trapezoidal integration failed.

4. CONCLUSIONS

We have shown that the Padé-Laplace method (18, 24) can be modified for analysis of fluorescence intensity decays detected by application of the multifrequency phase/modulation technique. The attractive feature of the method is that it indicates the number of exponential components and does not require initial guesses for the lifetime and fraction values. As an additional tool to this method we have proposed visual inspection of lifetime-fraction scattergrams. The MPL analysis of simulated data show that as many as four distinct components can be detected. The values of the lifetimes and fractions obtained by the MPL method are generally very close to those obtained by use of least-square fitting, procedures for both simulations and real data. Among the recoveries

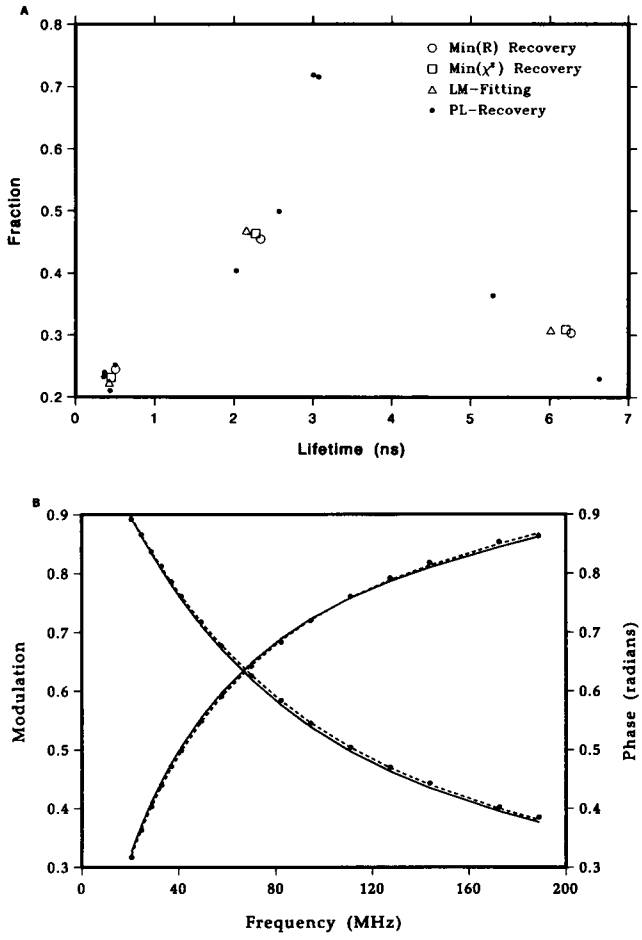

FIGURE 9 (*a*) The lifetime-fraction scattergram for 10 μM phospholipase A_2 in 20 mM MOPS at pH = 7.06. Excitation: 295 nm. Emission: 340-20. 16 phase/modulation data points were collected. Minimal frequency, 20.54 MHz, maximal frequency, 188.93 MHz. Method of integration: modified trapezoidal rule. $p_0 = 0.976$ ns^{-1}. Number of Padé approximants: 20, 7 satisfying $R < 0.05$.

Recovery	n	τ_k	f_k	χ_r^2	R
Min (R)	1	6.267	0.303		
	2	2.334	0.455		
	3	0.504	0.245	1.1×10^{-4}*	0.002
Min (χ^2)	1	6.200	0.309		
	2	2.272	0.463		
	3	0.449	0.232	6×10^{-5}	0.003
Average	1	6.234	0.306		
	2	2.303	0.459		
	3	0.476	0.238		
Average (16)	1	6.02 ± 0.43	0.320 ± 0.026		
	2	2.20 ± 0.14	0.458 ± 0.024		
	3	0.41 ± 0.04	0.224 ± 0.022	5×10^{-5}*	0.002
LM-fit	1	6.009	0.308		
	2	2.155	0.469		
	3	0.427	0.223	6×10^{-6}*	0
ISS-fit	1	6.04 ± 0.26	0.305 ± 0.025		
	2	2.16 ± 0.11	0.473 ± 0.017		
	3	0.42 ± 0.02	0.222	0.52	0

obtained from subsequent Padé approximants we found that the best are those for which χ_r^2 is minimal and/or the sum of fractions is closest to one. Unfortunately neither of these criteria proved conclusive. We have found cases for which better recovery corresponds to a substantially higher χ_r^2. This issue of the criteria for the best recovery of lifetimes and fractions deserves further examination. We have improved Padé-Laplace method by proposing a procedure for obtaining uncertainities in recovered parameters. The procedure is based on variation of the parameter p_0 around its optimal value and on choosing recoveries with minimal χ_r^2 as the "best" recoveries. In this way the MPL method is enriched by the elements of statistical procedures although it still represents a basically nonstatistical method. In our opinion a nonstatistical method for the analysis of multiexponential functions supports analyses obtained by statistical methods and it provides at least a good initial guess for subsequent use of least-square techniques. This is especially important when the ratio of lifetimes is close to 1. We found by simulations with a standard level of noise, that for two components, the lifetime ratio of 1.4 is the resolution limit for both MPL and standard methods.

It is apparent that the Padé-Laplace method can be improved in at least two ways. First, it may be possible to find a more accurate method for numerical integration of noisy functions. Second, improvement might also be achieved by use of other transformation procedures, e.g., through the use of a z-transform rather than the Laplace transform (18), particularly when only a small number of data points is available for analysis. The original PL method as developed by Yeramian and Claverie (18) was, after all, oriented primarily towards data that were essentially continuous in time.

An interesting issue is whether the MPL method is capable of distinguishing between discrete exponential and nonexponential fluorescence decays possibly described by continuous lifetime distributions. Our preliminary assessment suggests that the Padé-Laplace method applied to data simulated assuming bimodal Lorentzian distribution of lifetimes gave numerous and appreciably more scattered recoveries than those observed in discrete exponential simulations. Such response of the MPL method to nonexponential decay is to be expected as it indicates the absence of well-defined discrete exponential components. Once thoroughly examined and justified this capability of the MPL method to distinguish between

*χ^2 was not weighted, but the phase and the modulation are commensurable because the phase is expressed in radians. The estimated errors in lifetimes and fractions in LM-fit were of the order of 10^{-4} or less, which is probably unrealistic. (*b*) Phase/modulation data for as in *a* and theoretical curves obtained from average (16) recovery (*solid line*) and ISS-fit recovery (*dotted line*).

exponential and nonexponential decays will make it especially useful for fluorescence decay analysis.

On the basis of studies performed in this paper we conclude that at the present stage of its development modified Padé-Laplace method is complementary to other methods currently in use for the analysis of fluorescence decay.

APPENDIX

For the calculation of integral given in Eq. 18 and its derivatives with respect to p we use simple trapezoidal rule. It provides better results than the Simpson's rule in case of noisy integrands. If $\bar{C}(\omega_j)$ and $\bar{S}(\omega_j)$ are numerically given for $\omega_1, \ldots, \omega_m = \omega_{max}$, the integral in Eq. 18 is approximated by

$$\tilde{I}(p) \approx \frac{1}{\pi} \sum_{j=1}^{m} w_j \frac{p\bar{C}(\omega_j) + \omega_j \bar{S}(\omega_j)}{p^2 + \omega_j^2} + I_\infty(p)$$

$$w_j = (\omega_{j+1} - \omega_{j-1})/2, \quad j = 2, \ldots, m-1,$$

$$w_j = (\omega_j - \omega_{j-1})/2, \quad j = 1, m,$$

where $I_\infty(p)$ is the contribution of the tail part of integrand:

$$I_\infty(p) = \frac{1}{\pi} \int_{\omega_m}^{\infty} \frac{pC(\omega) + \omega S(\omega)}{p^2 + \omega^2} d\omega.$$

This contribution is evaluated by taking into account that the behavior of the intergrand for $\omega \to \infty$ is given by (see Eq. 14)

$$pC(\omega) + \omega S(\omega) = \sum_{k=1}^{n} \left(\frac{f_k p}{\tau_k^2 \omega^2 + 1} + \frac{f_k \tau_k}{\tau_k^2 + 1/\omega^2} \right) = r_1 + r_2/\omega^2 + r_3/\omega^4 + 0(\omega^{-8}),$$

where r_i, $i = 1, 2, 3$ are constant coefficients. Thus,

$$I_\infty(p) \approx (r_1 I_1 + r_2 I_2 + r_3 I_3)/\pi,$$

where $I_1 = [\pi/2 - arctg(\omega_m/p)]/p$, and

$$I_2 = (1/\omega_m - I_1)/p^2, \quad I_3 = [1/(3\omega_m^3) - I_2]/p^2.$$

The coefficients r_i are obtained by least square fitting of

$$(r_1 + r_2/\omega^2 + r_3/\omega^4)/(p^2 + \omega^2)$$

to the data for all ω, $\omega_c < \omega < \omega_{max}$, where ω_c is such that the integrand is monotonically decreasing for $\omega > \omega_c$.

In a completely analogous way we can evaluate the Taylor coefficients

$$d_i = \frac{(-1)^i}{i!} \frac{d^i}{dp^i} \tilde{I}(p).$$

(The differentiation and integration can be interchanged.) The behavior of the integrand for d_i when $\omega \to \infty$ is now given by:

$$(p^2 + \omega^2)^{-i/2 - 5/4 + (-1)^i/4} [r_{1i} + r_{2i}/\omega^2 + r_{3i}/\omega^4 + 0(\omega^{-8})], \quad i = 1, 2, 3, \ldots$$

Clearly, for higher order Taylor coefficients the contribution of the tail is less important.

Having described the numerical evaluation of $I_\infty(p)$, we now present another more sophisticated method for the numerical evaluation of the finite integration interval part of the integral 18:

$$\int_0^{\omega_m} \frac{pC(\omega) + \omega S(\omega)}{p^2 + \omega^2} d\omega. \tag{29}$$

The method may be called the "generalized trapezodial rule" because it is essentially the trapezoidal rule with nonlinear interpolation between two subsequent points. The integral 29 can be represented as a linear combination of the integrals of the following general form:

$$I = \int_a^b g(x) f(x)\, dx,$$

where $g(x)$ is defined for any $x \in [a, b]$, and $f(x)$ is defined at values $x_1, \ldots, x_m \in [a, b]$, $x_1 = a$, $x_m = b$ and it can be written as

$$f(x) = \sum_{k=1}^{n} v_k h(x, u_k).$$

Here v_k and u_k are unknown constants and $h(x, u)$ is defined for any $x \in [a, b]$ and any $u \in [u_{min}, u_{max}]$. In our specific case $f(x)$ is $C(\omega)$ or $S(\omega)$ as given by Eq. 14.

For $x \in [x_j, x_{j+1}]$, $j = 1, 2, \ldots, m-1$ we approximate $f(x)$ by one "dominant" component:

$$f(x) \approx \bar{v}_j h(x, \bar{u}_j), \quad f(x_j) = \bar{v}_j h(x_j, \bar{u}_j), \quad f(x_{j+1}) = \bar{v}_j h(x_{j+1}, \bar{u}_j).$$

From the last two equalities it follows:

$$f(x_j)/f(x_{j+1}) = h(x_j, \bar{u}_j)/h(x_{j+1}, \bar{u}_j), \quad j = 1, 2, \ldots, m-1.$$

We assume now that there is a unique solution of this equation for $\bar{u}_j$ which we will denote by

$$\bar{u}_j = F(x_j, x_{j+1}) \in [u_{min}, u_{max}].$$

In our specific case it is easy to find such solution. The unknown coefficient $\bar{v}_j$ is given by

$$\bar{v}_j = f(x_j)/h[x_j, F(x_j, x_{j+1})].$$

Using now the proposed one component approximation with explicitly evaluated $\bar{v}_j$ and $\bar{u}_j$, we arrive at the following approximation for the integral I

$$I \approx \sum_{j=1}^{m-1} w_j g(x_j) f(x_j), \quad w_j = \frac{\int_{x_j}^{x_{j+1}} g(x) h[x, F(x_j, x_{j+1})]\, dx}{g(x_j) h[x_j, F(x_j, x_{j+1})]}.$$

The integrals in this formula can be calculated numerically to the precision desired by the Gaussian, Romberg or any other quadrature algorithm or even by direct analytical evaluation if the functions $g(x)$ and $h(x, u)$ are suitable.

This manuscript is dedicated to the memory of Dr. P. Claverie who very generously assisted us in the early stages of the work.

We thank Dr. Joe Sharp whose help in dealing with statistical problems was very valuable. We also thank Peter Callahan and Ken Peters for their assistance with preparation of the figures, and Jill M. Smidt for typing the tables. In our Fortran program for the analysis by PL method we used the Harwell Subroutine Library (subroutines: MA21, PA06, QA04, VC03 and TG01).

The research was supported by the Mayo Foundation and by GM 34847 of the United States Public Health Service.

Received for publication 16 May 1988 and in final form 17 March 1989.

REFERENCES

1. O'Connor, D. V., and D. Phillips. 1984. Time-correlated Single Photon Counting. Academic Press, Inc., New York.
2. Wahl, P. H. 1975. Nanosecond Pulse Fluorimetry. In *New Techniques in Biophysics and Cell Biology*. Vol. 2. M. Pain and B. Smith, editors. John Wiley and Sons, Inc., Londong. 233–285.
3. Eisenfeld, J., and C. C. Ford. 1979. A systems-theory approach to the analysis of multiexponential fluorescence decay. *Biophys. J.* 26:73–84.
4. Ware, W. R. 1983. Time-resolved fluorescence spectroscopy in biochemistry and biology. *NATO ASI (Adv. Sci. Inst.) Ser. A. Life Sci.* 69:299–317.
5. Yguerabide, J. 1972. Nanosecond fluorescence spectroscopy of macromolecules. *Methods Enzymol.* 26:498–578.
6. Isenberg, I. 1983. Robust estimation in pulse-fluorometry, a study of the method of moments and least squares. *Biophys. J.* 43:141–148.
7. Spencer, R. D., and G. Weber. 1969. Measurement of subnanosecond fluorescence lifetimes with a cross-correlation phase fluorometer. *Ann. NY Acad. Sci.* 158:371–376.
8. Gratton, E., and M. Limkeman. 1983. A continuously variable frequency cross-correlation phase fluorometer with picosecond resolution. *Biophys. J.* 44:315–324.
9. Gratton, E., and R. Lopez-Delgado. 1980. Measuring fluorescence decay times by phase-shift and modulation using the high harmonic content of pulsed light sources. *Nuovo Cimento B.* 56:110–124.
10. Knutson, J. R., J. M. Beechem, and J. Brand. 1983. Simultaneous analysis of multiple fluorescence decays curves: a global approach. *Chem. Phys. Lett.* 102:501–507.
11. Beechem, J. M., J. R. Knutson, J. B. Ross, B. W. Turner, and L. Brand. 1983. Global resolution of heterogeneous decay by phase/modulation fluorometry: mixtures and proteins. *Biochemistry.* 22:6054–6058.
12. Beechem, J. M., M. Ameloot, and L. Brand. 1985. Global analysis of fluorescence decay surfaces: excited-state reactions. *Chem. Phys. Lett.* 120:466–472.
13. Beechem, J. M., and L. Brand. 1985. Time resolved fluorescence of proteins. *Annu. Rev. Biochem.* 54:43–71.
14. Ludescher, R. D., J. J. Wolwerk, G. H. de Haas, and B. S. Hudson. 1985. Complex photophysics of the single tryptophan of porcine pancreatic phospholipase A2, its zymogen and an enzyme/micelle complex. *Biochemistry.* 24:7240–7249.
15. Alcala, J. R., E. Gratton, and F. G. Prendergast. 1987. Interpretation of fluorescence decays in proteins using continuous lifetime distributions. *Biophys. J.* 51:925–936.
16. James, D. R., and W. R. Ware. 1985. Multiexponential fluorescence decay of indole-3-alkanoic acids. *J. Phys. Chem.* 89:5450–5458.
17. Livesey, A. K., and J. C. Brochon. 1987. Analyzing the distribution of decay constants in pulse-fluorometry using the maximum entropy method. *Biophys. J.* 52:693–706.
18. Yeramian, E., and P. Claverie. 1987. Analysis of multiexponential functions without hypothesis as to the number of components. *Nature (Lond.)* 326:169–174.
19. Baker, G. A., Jr. 1965. The theory and application of the Padé approximant method. *Adv. Theor. Phys.* 1:1–58.
20. Baker, G. A., Jr. 1973. The existence and convergence of subsequences of Padé approximants. *J. Math. Annal. Appl.* 43:498–528.
21. Gammel, J. L., and F. A. McDonald. 1966. Application of the Padé approximant to scattering theory. *Phys. Rev.* 142:1245–1254.
22. Zinn-Justin, J. 1971. Strong interaction dynamics with Padé approximants. *Phys. Rep.* 1:55–102.
23. Longman, I. M. 1971. Computation of the Padé table. *Int. J. Comp. Math.* 3:53–64.
24. Yeramian, E. 1986. Etude expérimentale et théorique de récepteurs de neuromédiateurs et déloppement de méthodologies pour l'analyse de signaux. Ph.D. thesis. Ecole Centrale des Arts et Manufactures, Chatenay Malabry, France.
25. Aubard, J., P. Levoir, A. Denis, and P. Claverie. 1987. Direct analysis of chemical relaxation signals by a method based on the combination of Laplace transform and Padé approximants. *Comput. Chem.* 11:163–178.
26. Bronshtein, I. N., and K. A. Semendyayev. 1985. *Handbook of Mathematics.* Van Nostrand Reinhold, New York. 581.
27. Bevington, R. P. 1969. Data Reduction and Error Analysis for the Physical Sciences. McGraw-Hill Book Co., New York.
28. Kempthorne, O., and L. Folks. 1971. Probability, Statistics and Data Analysis. Iowa State University Press, Ames, IA.
29. Alcala, J. R., E. Gratton, and D. M. Jameson. 1985. A multifrequency phase fluorometer using the harmonic content of a mode-locked laser. *Anal. Instrum.* 14:225–250.